TOPOGRAPHIC MAPPING OF THE MOON

M.T. Zuber
Department of Earth, Atmospheric and Planetary Sciences
Massachusetts Institute of Technology
Cambridge, MA 02139-4307
USA

D.E. Smith
Laboratory for Terrestrial Physics
Code 920
NASA/Goddard Space Flight Center
Greenbelt, MD 20771
USA

Commision IV, Working Group 5

KEY WORDS: DEM/DTM, extraterrestrial, mapping, electro-optical

ABSTRACT

We have processed laser altimetric data from the Clementine LIDAR to produce an accurate global model for the shape of the Moon. Ranges from the spacecraft to the lunar surface were converted to center of mass-referenced radii and expanded into a 72nd degree and order spherical harmonic model for lunar topography. Results show that the present shape of the Moon is a sphere with maximum positive and negative deviations of ~8 km, both occurring on the far in the areas of the Korolev and South Pole-Aitken basins. The near side has a gentle topography with an rms deviation of only about 1.4 km with respect to the best-fit sphere compared to the far side. The shapes of the histograms of the deviations from the sphere show a peaked distribution slightly skewed toward lower values for the near side, while the far side is broader but shows the South Pole-Aitken Basin as an anomaly compared to the rest of the hemisphere. Where Apollo and Clementine altimetry coverage overlap, measured relative topographic heights generally agree to within ~ 200 m, with most of the difference due to our more accurate orbit corrections for Clementine and to variations in large-scale urface roughness.

1 BACKGROUND

1.1 The Clementine Mission

The Clementine Mission, sponsored by the Ballistic Missile Defense Organization with science activities supported by NASA, mapped the Moon from February 19 through May 3, 1994 (Nozette et al. 1994). The spacecraft included a LIght Detection and Ranging (LIDAR) instrument that was built by Lawrence Livermore National Laboratory (Nozette et al. 1994). While the spacecraft was in orbit, this instrument was operated as a ranging device and collected near-globally distributed profiles of elevation round the Moon (Zuber et al. 1994). In this paper we discuss how data from the lementine LIDAR were processed to yield a global, geodetically-referenced model for the topography of the Moon.

1.2 Pre-Clementine Measurements of Lunar Topography

Measurements of lunar elevation have been derived from Earth-based and orbital observations. Earth-based measurements of lunar topography have necessarily been limited to the near side, and include limb profiles (Watts 1963), ground-based photogrammetry (Baldwin 1963; Hopmann 1967; Arthur and Bates 1968; Mills and Sudbury 1968) and radar interferometry (Zisk 1971; Zisk 1972). These studies yielded information of limited spatial distribution and positional knowledge of order 500 m.

Orbital data include landmark tracking by the Apollo command and service modules (Wollenhaupt et al. 1972), profiling by the Apollo long wavelength radar sounder (Brown et al. 1974), limb profiles from the Zond-6 orbiter (Rodionov et al. 1971) and photogrammetry from the Lunar Orbiters (Jones 1973). None of these observations was selenodetically referenced to the Moons center-of-mass, and all were characterized by absolute errors on the order of 500 m.

More accurate lunar shape information was derived from orbital laser ranging. The Apollo 15, 16 and 17 missions carried laser altimeters which provided measurements of the height of the command modules above the lunar surface (Kaula et al. 1972; Kaula et al. 1973; Kaula et al. 1974). These measurements provided the first information on the shape of the Moon in a center of mass reference frame.

2 LUNAR TOPOGRAPHIC MODEL

2.1 Measuring Lunar Topography

The Clementine LIDAR measured the slant range of the spacecraft to the lunar surface at spacecraft altitudes of 640 km or less. The instrument collected data for approximately one-half hour per 5-hour orbit for the two month lunar mapping mission. Specifications for the instrument are given in Table 1. For the first month, with spacecraft periselene at latitude -30^o, topographic profiles were obtained in the approximate latitude range -79^o to $+22^o$, while in the second month of mapping, with spacecraft periselene at latitude $+30^o$, profiles were obtained in the approximate range -20^o to $+81^o$.

To produce a global topographic dataset from the lidar system it was first necessary to subtract from the range profiles a precise orbit. We computed these orbits with the GEODYN/SOLVE orbital analysis programs (Putney 1977; McCarthy et al. 1994). We interpolated the spacecraft orbital trajectory to the time of the laser measurement, and then ac-

counted for the one-way light time to the surface to determine the selenocentric surface coordinates of the laser pulse. The timing of the arrival of the laser pulse on the lunar surface was converted to selenocentric coordinates by interpolating the spacecraft orbital trajectory to the time of the laser measurement and accounting for the one-way light time to the surface. We thus transformed the measured range from the spacecraft to the surface to a lunar radius in a center-of-mass reference frame. Our orbits were characterized by a formal uncertainty in radial position of about 10 m and have an accuracy with respect to the lunar center of mass of order 100 m, which is comparable to the single shot ranging precision of the lidar. The radial orbit accuracy determines to first order the accuracy of the global topographic model. We also included a correction for spacecraft pointing errors, which were at the milliradian level (Regeon et al. 1994), resulting in changes to measured ranges of up to 4 m.

The lidar typically ranged once per 1.6 sec, expending nearly a half million laser shots during the two month Clementine lunar mapping mission. The instrument detector triggered on 19% of the shots. To distinguish valid ranges from noise hits for these ~100,000 triggers, we applied a Kalman filter (Tarantola and Valette 1982) based on a stochastic model of topographic errors (Goff and Jordan 1988). We developed the filter (Zuber et al. 1996a) on the basis of the observation that planetary surface topography displays a fractal distribution (Turcotte 1987), which makes it possible to predict the likely dynamic range of topographic power over a specified spatial distance such as the along-track or cross-track laser shot spacing. Filtering the data yielded 72548 "valid" ranges.

2.2 Global Topographic Model

The filtered data were assembled into a 10.25^o x 0.25^o grid, corresponding to the minimum spacing between orbital passes. We note that most major lunar basins were sampled by Clementine altimetry. The LIDAR did not return much ranging information poleward of 78^o. Consequently, before performing a spherical harmonic expansion of the data set it was necessary to fill in the polar regions ($\sim$ 2% of the planets surface area) by interpolation. For this purpose we used the method of splines with tension (Smith and Wessel 1990) to continue the data smoothly across the poles. We then performed a 72^{nd} degree and order spherical harmonic expansion of the data to yield Goddard Lunar Topography Model-2 (GLTM-2) (Zuber et al. 1996a). The elevations were referenced to a spheroid with flattening of 1/3234.93, which corresponds to the flattening term, C_{20}, we obtained for the lunar gravity field (Lemoine et al. 1996). This is the observed dynamical flattening of the planet.

2.3 Fundamental Shape

To first order the present shape of the Moon is a sphere with maximum positive and negative deviations of $\sim$ 8 km, both occurring on the far side (240^oE, 10^oS; 160^oE, 75^oS) in the areas of the Korolev and South Pole-Aitken basins. These departures from sphericity are the combined result of various processes in the Moons early history (Zuber et al. 1996b). The two largest global-scale features are the center-of-mass/center-of-figure (COM/COF) offset and the polar flattening, both of which are of order 2 km. In addition there are smaller wavelength deviations, due primarily to impact basins. The power spectrum of the topographic shows more power at longer wavelengths as compared to previous models due to more complete sampling of the surface, particularly the far side basins. The power of topography follows a simple general relationship of 2 km/spherical harmonic degree.

Another fundamental characteristic of the lunar shape is that the topographic signatures of the near side and far side are very different. As shown in Figure 1, the near side has a gentle topography with an rms deviation of only about 1.4 km with respect to the best-fit sphere compared to the far side, which is twice as large. The shapes of the histograms of the deviations from the sphere show a peaked distribution slightly skewed toward lower values for the near side, while the far side is broader but clearly shows the massive far side South Pole-Aitken Basin as an anomaly compared to the rest of the hemisphere. The sharpness of the near side histogram is a result of the maria.

We compared elevations derived from the Clementine LIDAR to control point elevations from the Apollo laser altimeters (Davies et al. 1987). A summary of the attributes of the Clementine and Apollo data sets is presented in Table 2. Where Apollo and Clementine coverage overlap, measured relative topographic heights generally agree to within $\sim$ 200 m, with most of the difference due to our more accurate orbit corrections (Lemoine et al. 1995) and to variations in large-scale surface roughness (Zuber et al. 1996a). In contrast, Clementine topography often differs from landmark elevations on the lunar limb (Head et al. 1981) by as much as several km.

Differences in lunar shape parameters derived from Clementine vs. Apollo altimetry are mostly due to better coverage associated with the former: the greatest variations in lunar topographic height are on the far side over a broad latitude band, much of which was not sampled by the Apollo laser instruments.

Another notable charasteric of the Moon is the lack of any significant ellipticity in the equatorial plane. Figure 2 shows equatorial radii along with low degree and order spherical harmonic terms evaluated at the equator. The (2,2) terms in the spherical harmonic model indicate an amplitude in the equatorial plane of about 800 m with a maximum $\sim$ 40^oE longitude, smaller than the COM/COF offset, but aligned in the same general direction. In contrast, the Moons equatorial gravity field is aligned almost exactly with the Earth-Moon line. Figure 2 also illustrates that the (1,1) terms are more than a factor of two larger than the (2,2) terms, which indicates that the largest topographic effect around the lunar equator is the COM/COF offset.

3 REFERENCES

Arthur, D. W. G. and P. Bates 1968. The Tucson selenodetic triangulation. Commun. Luna Planet. Lab. 7, 313-361.

Baldwin, R. B. 1963. The Measure of the Moon, Ed., University of Chicago Press, Chicago, 88.

Brown, W. E. J., G. F. Adams, R. E. Eggleton, P. Jackson, R. Jordan, M. Kobrick, W. J. Peeples, R. J. Phillips, L. J. Porcello, G. Schaber, W. R. Sill, T. W. Thompson, S. H. Ward and J. S. Zelenka 1974. Elevation profiles of the Moon. Proc. Lunar Sci. Conf. 5th, 3037-3048.

Davies, M. E., T. R. Colvin and D. L. Meyer 1987. A Unified lunar control network: The near side. J. Geophys. Res. 92, 177-184.

Goff, J. A. and T. H. Jordan 1988. Stochastic modeling of seafloor morphology: Inversion of sea beam data for second-order statistics. J. Geophys. Res. 93, 13,589-13,608.

Head, J. W., E. Robinson and R. J. Phillips 1981. Topography of the Orientale basin. Lunar Planet. Sci. Conf. XII, 421-423.

Hopmann, J. 1967. General-Katalog absoluter Hohen auf dem Kond. Ann. Univ. Sternw. Wien 26, 7.

Jones, R. L. 1973. Estimates of the Moon's geometry using lunar orbiter imagery and Apollo laser altimeter data. NASA TR R-407.

Kaula, W. L., G. Schubert, R. E. Lingenfelter, W. L. Sjogren and W. R. Wollenhaupt 1974. Apollo laser altimetry and inferences as to lunar surface structure. Proc. Lunar Planet. Sci. Conf. 5, 3049-3058.

Kaula, W. M., G. Schubert, R. E. Lingenfelter, W. L. Sjogren and Wollenhaupt, W.R. 1973. Lunar topography from Apollo 15 and 16 laser altimetry. Proc. Lunar Sci. Conf. 4th, 2811-2819.

Kaula, W. M., G. Schubert, R. E. Lingenfelter, W. L. Sjogren and W. R. Wollenhaupt 1972. Analysis and interpretation of lunar laser altimetry. Proc. Lunar Sci. Conf. 3rd, 2189-2204.

Lemoine, F. G., D. E. Smith, M. T. Zuber, G. A. Neumann and D. D. Rowlands 1996. A 70th degree and order lunar gravity model from Clementine and historical data. J. Geophys. Res. submitted.

Lemoine, F. G., D. E. Smith, M. T. Zuber, D. D. Rpwlands and G. A. Neumann 1995. Results from the Clementine lunar geodesy investigation. Proc. Am. Astronaut. Soc. submitted.

McCarthy, J. J., S. Rowton, D. Moore, S. Luthcke, D. E. Pavlis, L. S. Tsaoussi, D. D. Rowlands and J. A. Marshall 1994. GEODYN Systems Descriptions and Operations Manuals, NASA GSFC and Hughes/STX Contractor Report.

Mills, G. A. and P. V. Sudbury 1968. Absolute coordinates of lunar features. Icarus 9, 538-561.

Nozette, S., P. L. Rustan, L. P. Plesance, D. M. Horan, P. Regeon, E. M. Shoemaker, P. D. Spudis, C. Acton, D. N. Baker, J. E. Blamont, B. B.J., M. P. Corson, M. E. Davies, T. C. Duxbury, E. M. Eliason, B. M. Jakosky, J. F. Kordas, I. T. Lewis, C. L. Lichtenberg, P. G. Lucey, E. Malaret, M. A. Massie, J. H. Resnick, C. J. Rollins, H. S. Park, A. S. McEwen, R. E. Priest, C. M. Pieters, R. A. Reisse, M. S. Robinson, R. A. Simpson, D. E. Smith, T. C. Sorenson, R. W. Vorder Bruegge and M. T. Zuber 1994. Clementine: Scientific overview. Science 266, 1835-1839.

Putney, B. H. 1977. General Theory for Dynamic Satellite Geodesy, NASA Spec. Publ., The National Geodetic Satellite Program.

Regeon, P. A., R. J. Chapman and R. Baugh 1994. Clementine: The Deep Space Program Science Experiment. Int. Acad. Astron. IAA-L-0501, 1-13.

Rodionov, B. N., I. V. Isavnina, Y. F. Avdeev, V. D. Glagov, A. F. Dorofeev, B. S. Dunaev, Y. L. Ziman, V. V. Kiselev, V. A. Krasikov, O. N. Lebedev, A. B. Makhailovskii, A. P. Tishchenko, B. V. Nepoklonov, V. K. Samoilov, F. M. Truskov, Y. M. Chesnokov and Y. I. Fivenskii 1971. New data on the Moon's figure and relief based on results from the reduction of Zond-6 photographs. Cosmic Res. 9, 410-417.

Smith, W. H. F. and P. Wessel 1990. Gridding with continuous curvature splines in tension. Geophysics 55.

Tarantola, A. and B. Valette 1982. Generalized nonlinear inverse problems solved using the least squares criterion. Rev. Geophys. Space Phys. 20, 219-232.

Turcotte, D. L. 1987. A fractal interpretation of topography and geoid spectra on the Earth, Moon, Venus and Mars. J. Geophys. Res. 92, E597-E601.

Watts, C. B. 1963. The marginal zone of the Moon. Astron. Papers Amer. Ephemer. Naut. Almanac 17.

Wollenhaupt, W. R., R. K. Osburn and G. A. Ransford 1972. Comments on the figure of the Moon from landmark tracking. The Moon 5, 149-157.

Zisk, S. H. 1971. A new, Earth-based radar technique for the the measurement of lunar topography, Conf. on Lunar Geophysics, Houston, 296-306.

Zisk, S. H. 1972. A new, Earth-based radar technique for the measurement of lunar topography. The Moon 4, 296-306.

Zuber, M. T., D. E. Smith, F. G. Lemoine and G. A. Neumann 1994. The shape and internal structure of the Moon from the Clementine mission. Science 266.

Zuber, M. T., D. E. Smith, G. A. Neumann and F. G. Lemoine 1996a. The topography of the Moon from the Clementine LIDAR. J. Geophys. Res.

Zuber, M. T., D. E. Smith, G. A. Neumann and F. G. Lemoine 1996b. What factors control the long wavelength shape of the Moon? Lunar Planet. Sci. Conf. XXVII, 1511-1512.

Table 1. Clementine LIDAR Instrument Parameters

Parameter	Value	Unit
Laser:		
type	Nd:YAG	
wavelength	1.064	mm
energy	171	mJ
beam divergence	500	mrad
nominal pulse repetition rate	0.6	Hz
Detector:		
type	SiAPD	
field of view	0.057	degrees
bandpass filter	0.4 to 1.1	mrad
Telescope:		
type	Cassegrain	
diameter	0.131	m
focal length	0.125	m
Receiver Electronics:		
clock counter	14	bits
frequency response	15.0001	MHz
return range bin	39.972	m
maximum range	640	km
gain	100x	
Other:		
spotsize at periselene	~200	m
assumed lunar albedo	0.15 to 0.5	
Instrument		
mass	2.370	kg
power	6.8 @ 1 Hz	W

Table 2. Comparison of Clementine Apollo Laser and Clementine LIDAR Profile Datasets

Parameters	Apollo	Clementine
Number of observations	7080	72,548
Coverage	-26° to +26°	-79° to 81°
Along-track resolution	30-43 km	~20 km
Across-track resolution	NA	~60 km
Single shot vertical resolution	2 m	39.972 m

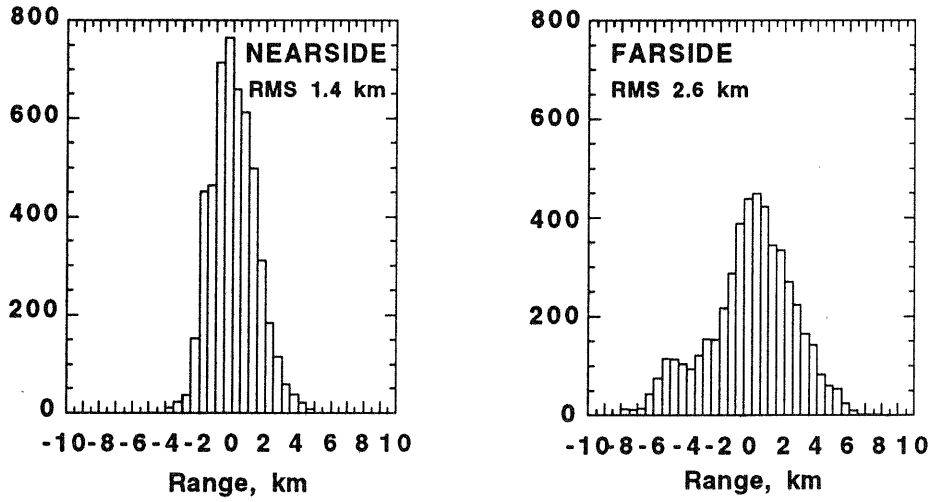

Figure 1. Histograms of the departure of the Moon from a sphere for the nearside and farside.

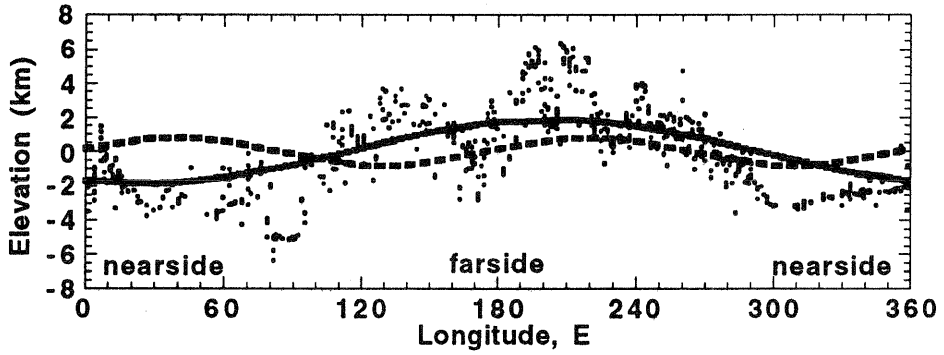

Figure 2. Lunar radii measured by Clementine within 1° of the equator. The values are subtracted from a mean of 1738.0 km. The solid line shows the (1,1) term of the spherical harmonic expansion of the topography and the dashed line shows the (2,2) term.